



The application of thermomicroscopy to the temperature programmed reduction in metal oxides

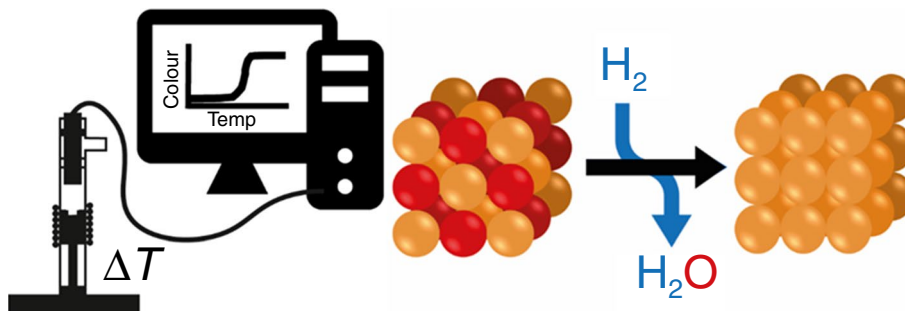
Gage P. Ashton¹ · Edward L. Charsley¹ · Lisa J. Gillie¹ · Lindsay P. Harding¹ · Gareth M. B. Parkes¹ · Adam J. Watson¹

Received: 16 August 2022 / Accepted: 12 March 2023 / Published online: 30 March 2023
© The Author(s) 2023

Abstract

Thermomicroscopy, or hot-stage microscopy, is primarily used in the analysis of organic materials such as pharmaceuticals and polymers. However, its potential application to the study of inorganic systems remains largely unexplored. A thermomicroscope was developed utilising red, green, blue (RGB) colour profiles and individual micrographs taken at fixed temperatures to follow temperature programmed reduction processes under a hydrogen atmosphere. The instrument was used for the study of the reduction in the oxides of silver, copper, lead, and cobalt. To the best of the authors' knowledge, this is the first time that temperature programmed reduction processes have been followed using thermomicroscopy and our results suggest the presence of transient intermediate phases within the lead oxide and cobalt oxide systems.

Graphical abstract



Keywords TPR · Thermomicroscopy · Hydrogen reduction · Metal oxides · Colour monitoring

Introduction

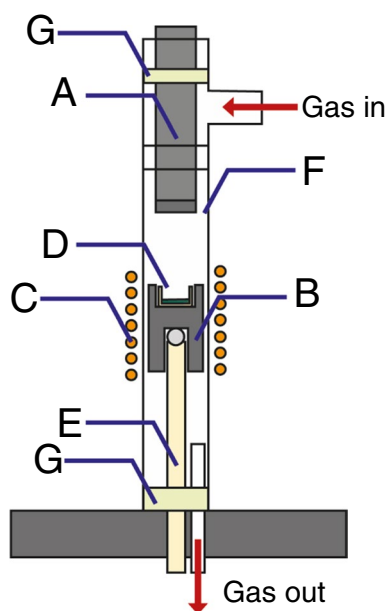
Temperature programmed reduction (TPR) is a thermoanalytical technique widely used to characterise both bulk and supported heterogeneous catalysts containing metal oxides [1, 2]. Typically, TPR is performed under an atmosphere of hydrogen, carbon monoxide or ammonia, usually blended with an inert gas such as nitrogen, helium, or argon [3–5].

In most cases, the TPR process is followed by evolved gas analysis (EGA) to monitor changes in the reductive gas concentration using a range of detectors such as thermal conductivity (TCD) [6], flame ionisation (FID) [7], photoionisation [8], and mass spectrometry (MS) [9]. The identification of reduction kinetic models is an area of particular interest [10–12].

Thermomicroscopy (sometimes referred to as hot-stage microscopy) studies the morphology and structural properties of materials optically as a function of temperature [13]. Thermomicroscopy can be performed in both reflected and transmitted modes. The latter technique is predominantly used for studying organic materials such as pharmaceuticals

✉ Gareth M. B. Parkes
g.m.b.parkes@hud.ac.uk

¹ Thermal Methods Research Unit, School of Applied Sciences, University of Huddersfield, Huddersfield HD1 3DH, UK



Scheme 1 TPR instrumentation developed and used for this study. **A** USB microscope, **B** iron stage, **C** induction coil, **D** sample crucible, **E** type K thermocouple, **F** ground glassware and **G** silicone gaskets

[14, 15], waxes [16, 17], and polymers [18, 19]. Reflected light techniques have been applied to a range of materials including inorganics [20, 21], glasses and ceramics [22, 23], high temperature sintering studies [24, 25], and crystal polymorphism [26, 27]. However, the use of thermomicroscopy with TPR remains largely undeveloped.

In this paper, we report the application of a newly developed thermomicroscopy instrument to the reflected light study of TPR on various metal oxide systems using colour profiling and micrographs.

Experimental

Instrumentation

Schematic 1 gives an overview of the instrument developed for this study. Briefly, the main body is constructed from ground glassware (**F**, 150 mm, 12 mm ID, 14/23 straight adapter) sealed with silicone gaskets (**G**) ensuring a low-volume gas-tight system. An induction circuit (**C**) provides non-contact heating of a stage (**B**), which comprises an iron rod (15 mm h, 10 mm d) with a cavity to hold a 5 mm ceramic crucible (**D**). Through the upper gasket, an endoscope style USB microscope (**A**, Oumij 2 MP) with an in-built focusing wheel is held securely in place focussing down on the sample crucible. The sample is illuminated with the microscope's in-built halo of LEDs. The temperature of the stage is measured using a type K thermocouple (**E**, 0.25 mm OD

wire) situated directly under the sample crucible within a twin bore alumina rod (2 mm OD).

Gas is passed into the top of the unit, via a mass flow controller (Brooks 5878) and exits through a port in the silicone gasket in the base of the instrument and passed directly into a Dreschel bottle containing water. Throughout this study, a flow rate of 30 mL min^{-1} of inert (N_2) or reductive gas (5% H_2 in N_2) was used.

Software

Software for instrument control and data acquisition was developed in house using Microsoft Visual Studio 2022. The software allows the control of the temperature, real-time image capture, and extraction of red, green, blue (RGB) colour values from regions of interest (ROI). Data are collected and stored as a comma separated variable (.csv) file, typically at a rate of once per second. The software supports a range of experiment types including the linear temperature programmes used in this study. Numerical data were processed using Microsoft Excel (365 edition) and plotted as a total RGB colour value as a function of temperature.

Materials

Nitrogen (99.998%, BOC) was used as an inert gas, and hydrogen in nitrogen (5% H_2 95% N_2 , BOC) was used for reduction experiments.

Temperature calibration of the instrument was achieved using high purity metals gallium (99.99%), indium (99.999%), tin (99.995%), lead (99.999%), zinc (99.99%) and aluminium (99.99%) all purchased from Goodfellow.

Samples of silver (I) oxide (Ag_2O , 99+%), silver (II) oxide (AgO , 99.9%), copper (II) oxide (CuO , 99.7%), copper hydroxycarbonate (*abbreviated to CuHC*, $\text{CuCO}_3 \cdot \text{Cu}(\text{OH})_2$, Cu 55% minimum), lead (IV) oxide (PbO_2 , 97%) and cobalt (II, III) oxide (Co_3O_4 , 99.7%) were all obtained from Alfa Aesar.

Methods

Temperature calibration

The temperature calibration was achieved through monitoring the optical changes in six metal samples (Ga, In, Sn, Pb, Zn, and Al) using a heating rate of 10 K min^{-1} to a temperature above the melting transition. All calibration experiments were performed under an inert atmosphere. During melting, the metallic surface relaxes and this is detected through a change in the RGB colour value, usually seen as a step (as

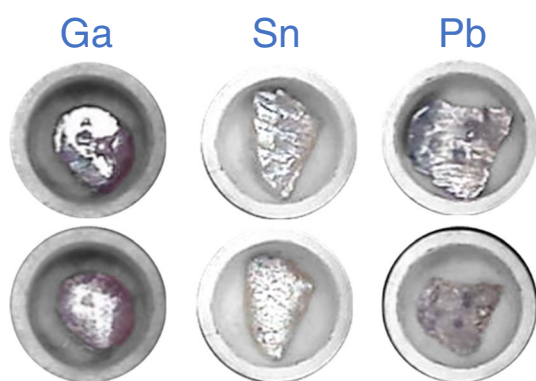
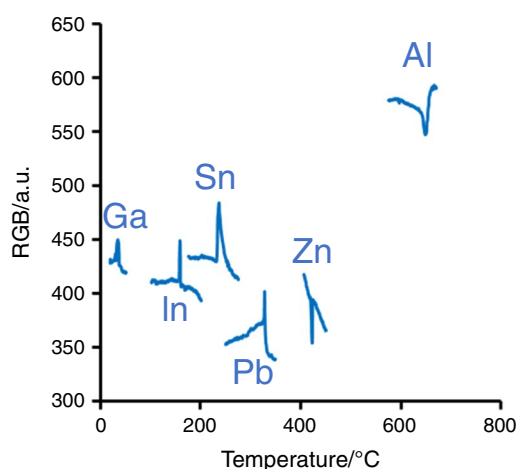


Fig. 1 Temperature calibration of the hot stage used in this study. The melting transitions of the metals; gallium (Ga), indium (In), tin (Sn), lead (Pb), zinc (Zn) and aluminium (Al) are observed as a total colour change (RGB) plotted as a function of temperature. Example micrographs are shown before (upper) and after (lower) the melt transition. (Sample mass: 5–35 mg; Heating rate: 10 K min⁻¹; Atmosphere: N₂, 30 mL min⁻¹)

shown in Fig. 1). The temperature of the transition is taken from the extrapolated onset of each step and used to generate a calibration graph using the values given in the International Temperature Scale of 1990 [29].

Silver (I) and (II) oxide

The effect of atmosphere on the decomposition/reduction in 10 mg samples of silver (I) oxide and silver (II) oxide was investigated using a heating rate of 10 K min⁻¹ between 30 and 500 °C.

Copper (II) oxide and CuHC

A comparison of the reduction and simultaneous decomposition/reduction in 10 mg samples of copper (II) oxide and

CuHC was investigated using a heating rate of 10 K min⁻¹ between 30 and 500 °C.

Lead (IV) oxide

The effect of atmosphere on the decomposition/reduction in 10 mg samples of lead (IV) oxide was investigated using a heating rate of 10 K min⁻¹ between 30 and 600 °C.

Cobalt (II, III) oxide

The effect of heating rate on the reduction in cobalt (II, III) oxide was studied using heating rates of 2.5, 5.0, 7.5 and 10.0 K min⁻¹ between 30 and 600 °C.

Results and discussion

Silver (I) and (II) oxide

The decomposition of silver (I) oxide under nitrogen is shown as a sharp step in the colour profile ($T_{\text{onset}} = 377$ °C) as the black oxide rapidly converts to silver metal (Fig. 2, upper, dashed line). The reduction process under 5% hydrogen is again shown as a step in the RGB colour profile (Fig. 2, upper, solid line) but at a much lower temperature ($T_{\text{onset}} = 158$ °C). Comparable results were obtained by Charsley et al. who used reflected light intensity measurement to follow the decomposition of silver (I) oxide [28]. Jelić et al. used thermogravimetry to study both the reduction and decomposition of silver (I) oxide. They also observed single step processes with the reduction occurring over a much lower temperature range of ~100 to 150 °C, notably lower than the decomposition which occurred at 380 °C [30].

The decomposition of silver (II) oxide under nitrogen is again shown as a step in the colour profile ($T_{\text{onset}} = 440$ °C) but at a higher temperature than for silver (I) oxide (Fig. 2, lower, dashed line). The reduction process under 5% hydrogen has a clear onset ($T_{\text{onset}} = 135$ °C) but occurs over a wider temperature range of ~150 °C (Fig. 2, lower, solid line). The low temperature and single stage nature of the reduction in silver (II) oxide has meant, and it has been used as a TPR calibration standard by some other workers [31, 32].

Selected micrographs of the two oxides under 5% hydrogen at 100, 200 and 300 °C are shown to demonstrate the overall change in colour.

Copper (II) oxide and CuHC

The RGB profiles for copper (II) oxide under inert and reducing atmospheres are shown in Fig. 3. The lack of change in the RGB colour profile is consistent with the

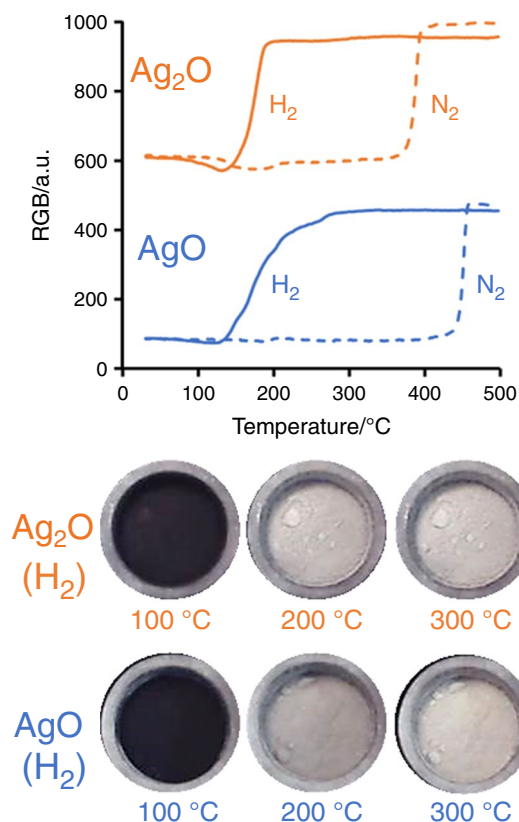


Fig. 2 Temperature programmed reduction (H_2 , solid line) and decomposition (N_2 , dashed line) of silver oxides (Ag_2O and AgO). Colour change profiles (RGB) are plotted as a function of temperature, the Ag_2O RGB colour profiles have been offset by 500 a.u. for clarity. Micrographs of the reduction in Ag_2O and AgO have been included along with their corresponding temperatures. (Sample mass: 10 mg, Heating rate: 10 K min^{-1} , Atmosphere: 30 mL min^{-1} of 5% H_2 in N_2 , or N_2 only)

stability of copper (II) oxide under nitrogen to $500\text{ }^\circ\text{C}$. Under 5% hydrogen the reduction is revealed as a step up in the colour profile ($T_{\text{onset}} = 348\text{ }^\circ\text{C}$) as the black oxide changes to the red copper metal as seen in the associated micrographs. Barnes et al. used a hygrometer to monitor the water produced during the reduction in copper (II) oxide under a 5% hydrogen in helium atmosphere. They also observed a similar single step profile under linear heating conditions of 5 K min^{-1} [33].

The RGB colour profile for $CuHC$ under nitrogen is shown by a step down ($T_{\text{onset}} = 195\text{ }^\circ\text{C}$) as the green salt decomposes to the black copper (II) oxide. Comparable results were obtained by Koga et al. who used TG–DTA to study the decomposition of a synthetic $CuHC$ (malachite) over a range of different heating rates [34].

The simultaneous decomposition/reduction experiment under 5% hydrogen has a more complex colour profile. Initially, the colour profile falls ($T_{\text{onset}} = 185\text{ }^\circ\text{C}$) as the salt decomposes, but then rises ($T_{\text{onset}} = 280\text{ }^\circ\text{C}$) as any oxides

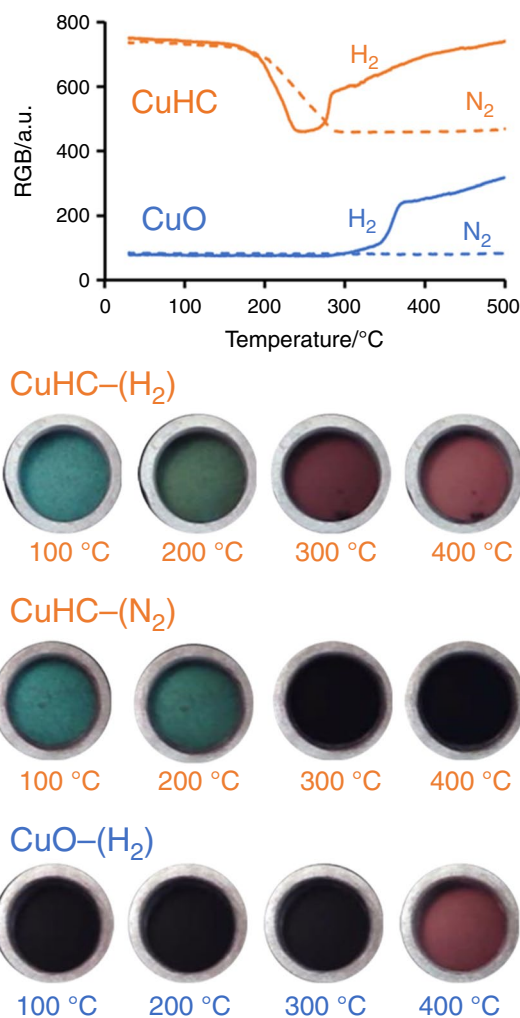


Fig. 3 Temperature programmed reduction (H_2 , solid line) and decomposition (N_2 , dashed line) of copper hydroxycarbonate ($CuHC$, $CuCO_3 \cdot Cu(OH)_2$) and copper oxide (CuO). Colour change profiles (RGB) are plotted as a function of temperature, and the $CuHC$ RGB colour profiles have been offset by 400 a.u. for clarity. Micrographs of the reduction in $CuHC$ and CuO , and the decomposition of $CuHC$ have been included along with their corresponding temperatures. (Sample mass: 10 mg, Heating rate: 10 K min^{-1} , Atmosphere: 30 mL min^{-1} of 5% H_2 in N_2 , or N_2 only)

formed are reduced to the copper metal. These colour changes can also be seen in the associated micrographs. Simultaneous decomposition/reduction experiments are less commonly performed but have been used in the preparation of supported catalysts [35].

Lead (IV) oxide

The behaviour of lead (IV) oxide under inert and reducing atmospheres over the temperature range $300\text{--}600\text{ }^\circ\text{C}$ is shown in Fig. 4. The decomposition of the black lead (IV) oxide to yellow lead (II) oxide is shown as a step in

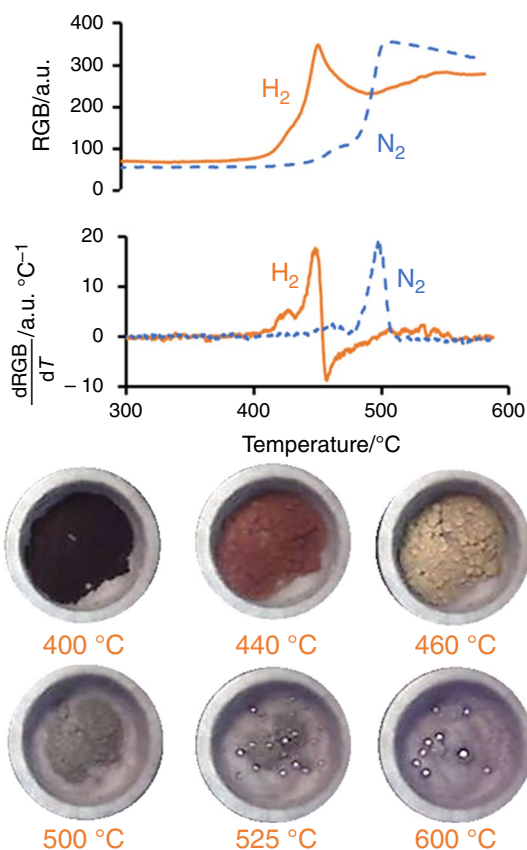


Fig. 4 Temperature programmed reduction (H_2 , solid line) and decomposition (N_2 , dashed line) of lead dioxide (PbO_2). Colour change profiles (RGB) and first derivatives ($d\text{RGB}/dT$) are plotted as a function of temperature. Selected micrographs and their corresponding temperatures have been included showing the reduction in lead dioxide. (Sample mass: 10 mg, Heating rate: 10 K min^{-1} , Atmosphere: 30 mL min^{-1} of 5% H_2 in N_2 , or N_2 only)

the colour profile ($T_{\text{onset}} = 477^\circ\text{C}$) and a peak in the differential colour profile. Karski and Paryjczak used a katharometer to study the TPR of lead and palladium oxides supported on alumina using 8% hydrogen in argon. They found that the pure lead oxide reduction was completed by 600 $^\circ\text{C}$ but was at a lower temperature when supported on alumina [36].

The reduction in lead (IV) oxide under 5% hydrogen gives rise to a more complex colour profile with an earlier onset temperature ($T_{\text{onset}} = 432^\circ\text{C}$). The differential colour profile indicates a two-stage process, and this is supported by the micrographs with a red–orange intermediate (tentatively assigned to lead (II, IV) oxide) being formed around 440 $^\circ\text{C}$. This quickly converts to the yellow oxide similar to that observed under nitrogen. The reduction in this oxide proceeds to liquid elemental lead, as seen in the micrographs as a series of beads forming above 500 $^\circ\text{C}$. This experiment shows the potential benefit of optical

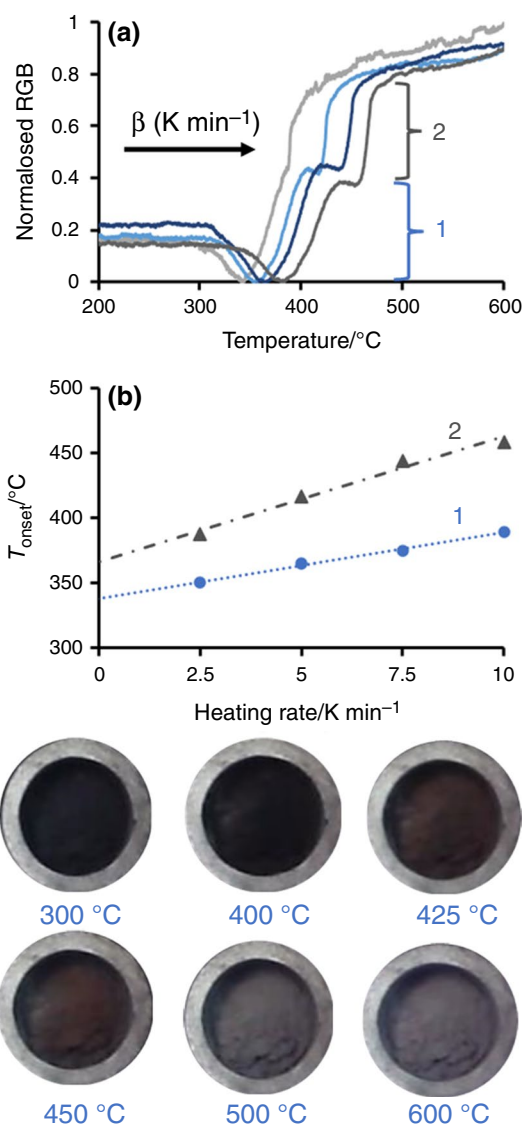


Fig. 5 Temperature programmed reduction in cobalt oxide (Co_3O_4). Normalised colour change profile plotted as a function of temperature at various heating rates (A). Heating rate dependency profile (B) for the onset of reduction in step one (1) and step (2). Selected micrographs and their corresponding temperatures have been included for the reduction in cobalt oxide at 10 K min^{-1} . (Sample mass: 10 mg, Heating rate: 2.5, 5.0, 7.5 and 10 K min^{-1} , Atmosphere: 30 mL min^{-1} of 5% H_2 in N_2)

monitoring of reduction processes, in that transient species can be observed that may be difficult to detect using other thermal techniques.

Cobalt (II, III) oxide

The effect of four heating rates on the reduction in cobalt (II, III) oxide is shown in Fig. 5A as normalised colour profiles. All profiles are similar having an initial decrease starting around 300 $^\circ\text{C}$ followed by a two-stage increase up to

600 °C. The resolution between steps (1 and 2) increases with heating rate. The associated micrographs from the 10 K min⁻¹ experiment show that the colour changes throughout the reduction are quite subtle (black to grey); however, the RGB colour profile is still able to distinguish the two steps. In addition, from the micrographs at 425 °C and 450 °C, a red-brown phase is apparent between steps 1 and 2, a colour not normally associated with cobalt oxides.

The onsets of steps 1 and 2 are plotted against heating rate (Fig. 5B). This allows the thermodynamic transition temperatures at zero heating rate to be determined via extrapolation in a similar manner to that widely used in DSC studies [37]. The extrapolated value of step 1 was found to be 335 °C, and step 2 was found to be 369 °C at a 0 K min⁻¹ heating rate.

Mishra et al. studied the reduction in cobalt (II, III) oxide using low temperature hydrogen plasma and reported that the process occurs via two stages: $\text{Co}_3\text{O}_4 \rightarrow \text{CoO} \rightarrow \text{Co}$ [38]. Bulvachenko et al. studied the reduction in pure and supported cobalt (II, III) in a 10% hydrogen atmosphere and observed a similar two-stage process [39]. Zhang and co-workers looked at the effect of water vapour on the reduction in supported cobalt oxide catalysts in 5% hydrogen in argon. Their results also suggested that the reduction occurred in two stages, but found that water vapour significantly affects the process [40].

The reduction process occurs faster at higher heating rates thus leading to a decrease in hydrogen concentration around the sample and a corresponding increase in the resolution between steps 1 and 2. The experimental results suggest that a three-stage process may occur, in contrast to previous authors, but further work is required to confirm and identify the intermediate oxide.

Conclusions

A thermomicroscope was constructed to allow the study of temperature programmed reduction processes, through micrographs and colour profiles of metal oxides under different atmospheres up to 600 °C.

Comparisons were made of the behaviour of a range of metal oxides heated under nitrogen and 5% hydrogen atmospheres which demonstrated that the colour profile is a viable method for monitoring reaction processes. As many metal oxides are highly coloured, thermomicroscopy may offer an advantage in detecting the presence of transient intermediates, which could be missed by other thermal methods.

Further work will incorporate a mass spectrometer to the thermomicroscope system, tracking the hydrogen concentration and this will be correlated with the colour profiles observed. In addition, the mass spectrometer will allow the study of complex decomposition processes.

Most TPR experiments use linear heating programmes; however, this can lead to issues in non-uniformity of conditions, particularly as a result in the change of the concentration of the reductive gas. This effect was noted in the cobalt (II, III) oxide system where a two-step process was more pronounced at higher heating rates. A follow-up study plans to explore the use of sample controlled thermal analysis (SCTA) where the temperature profile is adjusted to ensure processes occur at a constant low rate [29, 41].

Author contributions GPA was contributed to investigation, conceptualisation, formal analysis, writing—original draft, writing—review and editing; ELC was contributed to conceptualisation, writing—review and editing; LJG was contributed to writing—review and editing; LPH was contributed to supervision, writing—review and editing; GMBP was contributed to conceptualisation, formal analysis, supervision, writing—original draft, writing—review and editing; AJW was contributed to investigation, conceptualisation, formal analysis.

Open Access This article is licensed under a Creative Commons Attribution 4.0 International License, which permits use, sharing, adaptation, distribution and reproduction in any medium or format, as long as you give appropriate credit to the original author(s) and the source, provide a link to the Creative Commons licence, and indicate if changes were made. The images or other third party material in this article are included in the article's Creative Commons licence, unless indicated otherwise in a credit line to the material. If material is not included in the article's Creative Commons licence and your intended use is not permitted by statutory regulation or exceeds the permitted use, you will need to obtain permission directly from the copyright holder. To view a copy of this licence, visit <http://creativecommons.org/licenses/by/4.0/>.

References

1. Pirola C, Galli F, Patience GS. Experimental methods in chemical engineering: temperature programmed reduction—TPR. *Can J Chem Eng.* 2018;96:2317–20.
2. Da Ros S, Flores KAV, Schwaab M, Barbosa-Coutinho E, Fernandes NRC, Pinto JC. Phenomenological approaches for quantitative temperature-programmed reduction (TPR) and desorption (TPD) analysis. *J Ind Eng Chem.* 2021;94:425–34.
3. Reiche MA, Maciejewski M, Baiker A. Characterization by temperature programmed reduction. *Catal Today.* 2000;56:347–55.
4. Jin Y, Datye AK. Phase transformations in iron Fischer-Tropsch catalysts during temperature-programmed reduction. *J Catal.* 2000;196:8–17.
5. Nanba T, Masukawa S, Uchisawa J, Obuchi A. Characterization of Cu species on SiO₂ and ZSM-5 by temperature-programmed reduction by ammonia. *J Therm Anal Calorim.* 2013;113:793–802.
6. Lup ANK, Abnisa F, Daud WMAW, Aroua MK. Temperature-programmed reduction of silver(I) oxide using a titania-supported silver catalyst under a H₂ atmosphere. *J Chin Chem Soc.* 2019;66:1443–55.
7. Einemann M, Neumann F, Thomé AG, Wabo SG, Roessner F. Quantitative study of the oxidation state of iron-based catalysts by inverse temperature-programmed reduction and its

- consequences for catalyst activation and performance in Fischer-Tropsch reaction. *Appl Catal A Gen.* 2020;602:117718.
8. Afanasiev P. On the interpretation of temperature programmed reduction patterns of transition metals sulphides. *Appl Catal A.* 2006;303:110–5.
 9. Barnes PA, Parkes GMB, Brown DR, Charsley EL. Applications of new high resolution evolved-gas analysis systems for the characterisation of catalysts using rate-controlled thermal analysis. *Thermochim Acta.* 1995;269–270:665–76.
 10. Li CE, Wong L, Tang L, Scarlett NVY, Chiang K, Patel J, Burke N, Sage V. Kinetic modelling of temperature-programmed reduction of cobalt oxide by hydrogen. *Appl Catal A Gen.* 2017;537:1–11.
 11. Tiernan MJ, Barnes PA, Parkes GMB. The investigation of kinetic parameters using rate perturbation and linear heating thermoanalytical techniques. *J Phys Chem B.* 2001;105:220–8.
 12. Heidebrecht P, Galvita V, Sundmacher K. An alternative method for parameter identification from temperature programmed reduction (TPR) data. *Chem Eng Sci.* 2008;63:4776–88.
 13. Wiedemann HG, Felder-Casagrande S. Chapter 10 - thermomicroscopy. In: Brown ME, editor. *Handbook of thermal analysis and calorimetry.* London: Elsevier; 1998. p. 473–97.
 14. Drozd KV, Manin AN, Boycov DE, Churakov AV, Perlovich GL. Pharmaceutical multicomponent crystals of antifungal drugs with improved dissolution performance. *Cryst Growth Des.* 2021;21:7285–97.
 15. Perpétuo GL, Chierice GO, Ferreira LT, Fraga-Silva TFC, Venturini J, Arruda MSP, Bannach G, Castro RAE. A combined approach using differential scanning calorimetry with polarized light thermomicroscopy in the investigation of ketoprofen and nicotinamide cocrystal. *Thermochim Acta.* 2017;651:1–10.
 16. Létóffé JM, Claudy P, Kok MV, Garcin M, Volle JL. Crude oils: characterization of waxes precipitated on cooling by d.s.c. and thermomicroscopy. *Fuel.* 1995;74:810–7.
 17. Japper-Jaafar A, Bhaskoro PT, Mior ZS. A new perspective on the measurements of wax appearance temperature: comparison between DSC, thermomicroscopy and rheometry and the cooling rate effects. *J Petrol Sci Eng.* 2016;147:672–81.
 18. Ashton GP, Charsley EL, Harding LP, Parkes GMB. Applications of a simultaneous differential scanning calorimetry–thermomicroscopy system. *J Therm Anal Calorim.* 2022;147:1345–53.
 19. Kozyra A, Mugheirbi NA, Paluch KJ, Garbacz G, Tajber L. Phase diagrams of polymer-dispersed liquid crystal systems of itraconazole/component immiscibility induced by molecular anisotropy. *Mol Pharm.* 2018;15:5192–206.
 20. Charsley EL, Kamp ACF. A versatile hot stage microscope unit. In: Wiedemann HG, editors. *Advances in instrumentation.* Birkhäuser Basel: Basel; 1972. p. 499–513.
 21. Haines PJ. Simultaneous differential scanning calorimetry and reflected light intensity (DSC–RLI) in the study of inorganic materials. *Thermochim Acta.* 1999;340–341:285–92.
 22. Salem S, Jazayeri SH, Bondioli F, Allahverdi A, Shirvani M. Characterizing thermal behavior of ceramic glaze containing nano-sized cobalt-aluminate pigment by hot stage microscopy. *Thermochim Acta.* 2011;521:191–6.
 23. Ludwig M, Śnieżek E, Jastrzębska I, Prorok R, Li Y, Liao N, Nath M, Vlček J, Szczerba J. Corrosion resistance of MgO and Cr₂O₃-Based refractory raw materials to PbO-Rich Cu slag determined by hot-stage microscopy and pellet corrosion test. *Materials.* 2022;15:725.
 24. Enríquez E, Fuertes V, Cabrera MJ, Seores J, Muñoz D, Galiana B, Fernández JF. Study of the crystallization in fast sintered Na-rich plagioclase glass-ceramic. *Ceram Int.* 2019;45:8899–907.
 25. Panna W, Wyszomirski P, Kohut P. Application of hot-stage microscopy to evaluating sample morphology changes on heating. *J Therm Anal Calorim.* 2016;125:1053–9.
 26. Grivel JC, Guevara MJS, Zhao Y, Tang X, Pallewatta PGAP, Bednarčík J, Watenphul A. Thermal behavior and decomposition of cerium(III) butanoate, pentanoate and hexanoate salts upon heating in argon. *J Anal Appl Pyrol.* 2017;126:77–87.
 27. Neumann T, Jess I, Germann LS, Dinnebier RE, Näther C. Trimorphism of Zn(NCS)₂(4-dimethylaminopyridine)₂: crystal structures, thermodynamic relations, and comparison with the Co(II) polymorphs. *Cryst Growth Des.* 2019;19:1134–43.
 28. Preston-Thomas H. International Temperature Scale of 1990 (ITS-90). *Metrologia.* 1990;27:3–10.
 29. Charsley EL, Stewart C, Barnes PA, Parkes GMB. Development and applications of sample controlled thermomicroscopy. *J Therm Anal Calorim.* 2003;72:1087–90.
 30. Jelić D, Penavin-Škundrić J, Majstorović D, Mentus S. The thermogravimetric study of silver(I) oxide reduction by hydrogen. *Thermochim Acta.* 2011;526:252–6.
 31. Kuhn JN, Ozkan US. Effect of Co content upon the bulk structure of Sr- and Co-doped LaFeO₃. *Catal Lett.* 2008;121:179–88.
 32. Ma Y, Ma Y, Zhao Z, Ma S, Meng Q, Hu X, Buckley CE, Dong D. Fibrous La₂Zr₂O₇ pyrochlore-supported Ni nanocatalysts for methane reforming. *J Phys Chem Solids.* 2020;147: 109643.
 33. Barnes PA, Tiernan MJ, Parkes GMB. Sample controlled thermal analysis temperature programmed reduction of bulk and supported copper oxide. *J Therm Anal Calorim.* 1999;56:733–7.
 34. Koga N, Criado JM, Tanaka H. Apparent kinetic behavior of the thermal decomposition of synthetic malachite. *Thermochim Acta.* 1999;340–341:387–94.
 35. Al-Dalama K, Stanislaus A. Temperature programmed reduction of SiO₂–Al₂O₃ supported Ni, Mo and NiMo catalysts prepared with EDTA. *Thermochimica Acta.* 2011;520:67–74.
 36. Karski S, Paryjczak T. Investigation of Pd–Pb/Al₂O₃ catalysts by temperature-programmed reduction. *React Kinet Catal Lett.* 1981;15:419–24.
 37. Charsley EL, Laye PG, Markham HM, Hill JO, Berger B, Griffiths TT. Determination of the equilibrium temperatures and enthalpies of the solid–solid transitions of rubidium nitrate by differential scanning calorimetry. *Thermochim Acta.* 2008;469:65–70.
 38. Sabat KC, Paramguru RK, Pradhan S, Mishra BK. Reduction of cobalt oxide (Co₃O₄) by low temperature hydrogen plasma. *Plasma Chem Plasma Process.* 2015;35:387–99.
 39. Bulavchenko OA, Cherepanova SV, Malakhov VV, Dovlitova LS, Ishchenko AV, Tsybulya SV. In situ XRD study of nanocrystalline cobalt oxide reduction. *Kinet Catal.* 2009;50:192–8.
 40. Zhang Y, Wei D, Hammache S, Goodwin JG. Effect of water vapor on the reduction of Ru-promoted Co/Al₂O₃. *J Catal.* 1999;188:281–90.
 41. Parkes GMB, Charsley EL. Chapter 11 - sample controlled thermal analysis. In: Gaisford S, Kett V, Haines PJ editors. *Principles thermal analysis and calorimetry*, 2nd edn. Royal Society of Chemistry; 2016. p. 232–257.

Publisher's Note Springer Nature remains neutral with regard to jurisdictional claims in published maps and institutional affiliations.